Landslides (2022) 19:1957–1970
DOI 10.1007/s10346-022-01904-9
Received: 14 December 2021
Accepted: 12 May 2022
Published online: 26 May 2022

Wenkai Feng · Huilin Bai · Bing Lan · Yiying Wu · Zhongteng Wu · Liangzheng Yan · Xinjun Ma

Spatial–temporal distribution and failure mechanism of group-occurring landslides in Mibei village, Longchuan County, Guangdong, China

Abstract From June 10 to 13, 2019, continuous heavy rainfall occurred in Longchuan County, Guangdong Province, yielding a cumulative rainfall of nearly 270 mm. The heavy rainfall triggered a large number of landslide disasters and formed three hardest-hit areas. In this paper, Mibei village, Beiling town, Longchuan County, is chosen as the research object; detailed field investigation data, satellite remote sensing images, rainfall monitoring data, and artificial rainfall physical model test results are integrated; the temporal and spatial distribution characteristics of rainfall-induced group-occurring landslides in the study area are obtained; and the rainfall instability mechanism of granite residual soil slopes is explained. Under the influence of continuous heavy rainfall from June 10 to 13, 2019, 327 landslides developed in Mibei village, Beiling town, and these landslides were mainly distributed in low mountainous areas, of which the sections at elevations from 300 ~ 400 m and slopes ranging from 35 ~ 45° were the most susceptible to landslide disasters. Continuous rainfall on June 10 and 11 was the controlling factor leading to these large number of landslides, with numerous landslides occurring from 20:00 on June 11 to 04:00 on June 13. These group-occurring landslides exhibited the characteristics of a considerable rainfall lag. The deformation and failure characteristics of the numerous observed landslides within the study area were highly similar, mainly involving traction sliding failure, and the sliding mass thickness ranged mostly from 1.5 ~ 3 m. The flow pattern characteristics of unconsolidated deposits after landslide instability were significant. According to the deformation and failure characteristics of landslides and the rainfall infiltration pattern, the development of landslides was divided into stages in this paper. Due to the difference between the rainfall intensity and permeability of granite residual soil, the main influence depth of heavy rainfall was limited to the superficial zone of slopes, which is the main reason why the shallow surface zone was damaged by landslides. Under the action of continuous heavy rainfall, a saturated seepage field was established in the shallow surface zone of slopes. Driven by gravitational potential energy, this led to an uneven distribution of the slope saturation zone. Attenuation of the mechanical strength of saturated soil reduced the slope stability, and sliding failure consequently occurred in the shallow surface saturation zone. In regard to excavated slopes, anti-sliding force reduction and free face formation enhanced the slope's susceptibility to sliding failure under the influence of heavy rainfall, which is also the reason for the large-scale distribution of landslides along the X158 county road.

Keywords Granite residual soil · Temporal and spatial distribution characteristics · Continuous heavy rainfall · Group-occurring landslides · Failure mechanism

Introduction

Granite layers comprise one of the most typical strata in the southeast coastal provinces of China. Granite produces widely distributed residual soil layers under long-term weathering. Affected by the regional subtropical monsoon climate, typhoons frequently occur from May to October. Heavy rainfall in areas impacted by typhoons often leads to large-scale landslide disasters. In granite-dominated areas, controlled by the properties of granite-derived residual soil and slope structure characteristics, the incidence of group-occurring landslides in the superficial zone of granite residual soil slopes has become a very prominent phenomenon. This type of landslide moves along the residual layer, with a shallow sliding surface, small scale, and limited impact of a single disaster. However, large-scale group-occurring characteristics can cause notable life and property losses (Luo et al. 2014; Liu et al. 2016; Yang et al. 2020).

According to statistics, during the 10-year period from 2012 to 2021, many rainfall-induced group-occurring landslide disasters occurred in the southeastern coastal provinces of China. For example, the heavy rainfall attributed to super typhoon *Soudelor* caused large-scale disasters in many counties and cities across Zhejiang Province in 2015, resulting in many deaths, and hundreds of thousands of people were affected (Liu et al. 2018). In 2019, heavy rainfall generated mountain torrents and produced a large number of landslides and debris flows in Lingyun County, Guangxi Province, resulting in 14 deaths or missing people and serious damage to buildings and facilities along the flood flow path (Ding et al. 2020). In 2019, group-occurring landslides and debris flows caused by heavy rainfall occurred in many areas in Fujian Province, causing serious losses in Pucheng County and Sanming city of Fujian (Yang et al. 2021). From the perspective of geological environmental conditions, factors such as heavy rainfall, topography, granite residual soil properties, and slope structure play an important role in disaster events. Among these factors, rainfall is the main influencing factor of group-occurring landslides, while the other factors that constitute the internal conditions determine whether a disaster occurs, which comprehensively leads to the phenomenon of group-occurring

landslides in granite areas (Li et al. 2020; Liu et al. 2020a, b; Gutierrez-Martin 2020). In terms of research results on rainfall-induced landslides, a large number of scholars have studied the mechanical characteristics and attenuation pattern of granite residual soil from the perspectives of volumetric moisture content, clay content, and dry–wet cycle conditions. With increasing volumetric moisture content and number of dry–wet cycles, a continuous attenuation trend of the soil strength has been widely confirmed (An et al. 2020; Chen et al. 2011; Jian et al. 2017; Wen et al. 2016; Liu et al. 2019; Yi et al. 2021). Scholars have employed numerical simulation technology and permeability tests to determine the characteristics and evolution of the seepage field in granite residual soil slopes under rainfall and have established applicable seepage models (Liu et al. 2020a, b; Jian et al. 2020; Pan et al. 2020; Herrada et al. 2014; Gutierrez-Martin et al. 2021). Wang (2011) evaluated the stability of granite residual soil slopes through physical simulation tests and developed a slope stability evaluation model based on support vector machine theory. Xu (2015) performed physical model tests on different slopes; monitored the moisture content, soil pressure, and matrix suction during rainfall; obtained the characteristics of the whole slope instability process under rainfall; and preliminarily explained the instability mechanism of granite residual soil slopes.

After systematically combining existing research results, the authors found that the research results on granite residual soil slope disasters more notably focus on soil physical and mechanical properties, the research angle is biased toward basic research, and disaster-related studies remain lacking, especially model tests of the original slope structure. After participating in emergency rescue and treatment activities in Mibei village, Beiling town, Longchuan County, Guangdong Province, in 2019, the research group obtained details of group-occurring landslides in Mibei village, comprehensively collected rainfall monitoring data, optical satellite remote sensing images, and other data and completed a series of data analyses and tests. Based on a large number of previous studies, in this paper, the temporal and spatial distribution characteristics of group-occurring landslides are first analyzed based on the overall disaster situation in the study area, and the disaster mechanism of granite residual soil slopes is subsequently studied through artificial rainfall physical model tests combined with typical cases.

Overview of the disaster event

Longchuan County is subordinate to Heyuan city, Guangdong Province, and is located in northeastern Guangdong Province and borders Jiangxi Province. From June 10 to 13, 2019, sudden and continuous heavy rainfall occurred in Longchuan County, with a cumulative rainfall amount of nearly 270 mm and a maximum hourly rainfall amount of nearly 50 mm. A new rainfall intensity record was set. Heavy rainfall lasting for 4 days resulted in a large number of landslides across the county, which exhibited a centralized distribution, yielding three hardest-hit areas, including Mibei village in Beiling town (Fig. 1), Shangxi village in Mabugang town, and Banjing village in Xi'ao town, with direct economic losses reaching up to 1.545 billion yuan.

Mibei village, Beiling town, is located in the northernmost part of Longchuan County. Under the influence of the abovementioned continuous heavy rainfall, hundreds of small landslides occurred, which were distributed near roads, houses, and gullies, resulting in 7.2 km of road damage, direct damage to 4 houses, and more than 50 houses impacted. The economic loss in Mibei village alone reached as high as 120 million yuan (Bai et al. 2021). After the second day of heavy rainfall, the local government issued meteorological early warning information in a timely manner and transferred 377 residents in advance, and no casualties consequently occurred in Mibei village. After the disaster, the research group immediately engaged in rescue activities, focusing on the hardest-hit area of Mibei village, Beiling town. From June to November 2019, the research group successively completed rescue, postdisaster recovery, and treatment activities in the hardest-hit area of Mibei village, Beiling town. As such, the research group is very familiar with the overall geological environment characteristics and disaster conditions in Mibei village. Hourly rainfall monitoring data pertaining to Mibei village were collected from June 9 to 13, 2019, and daily rainfall data from May to July and monthly rainfall data from 1998 to 2018 were

Fig. 1 Unmanned aerial vehicle image after the disaster in Mibei village, Beiling town

further acquired. Moreover, two phases of remote sensing images in January and August 2019 were obtained from Google Earth. Abundant basic data were thus required in this study. Therefore, the hardest-hit area of Mibei village, Beiling town, was selected as the research object in this study.

Geo-environmental conditions

The study area exhibits a low mountainous and hilly terrain. In the study area, the terrain is generally high in the north and south and low at the center. Figure 2 shows the topographic characteristics of the study area. The highest altitude in the area is 609 m, and the lowest altitude reaches 183 m, which occurs at the outlet of the lower reaches of the Mibei River. The Mibei River is a secondary tributary of the Dongjiang River. The river channel is approximately 5 ~ 8 m wide and 4.1 km long. The flow pattern changes notably with the season. This river is the main water source for local irrigation. The northern Mibei River is dominated by low mountains. At the early stage, surface water undercutting erosion formed steep slopes on both sides of the channel, with a slope ranging from 35 ~ 45° and local slopes higher than 50°. However, the channel is narrow and mostly exhibits a V-shaped channel section. The southern Mibei River is located in an area with a mainly hilly terrain, with gradual topographic relief. The top of hills is mostly rounded, and the topographic slope decreases to 20 ~ 35°. The terrain along the Mibei River is relatively flat and is the main gathering area hosting cultivated land. In this area, alternating distribution patterns of low mountains, valleys, and hilly terrains can be observed from

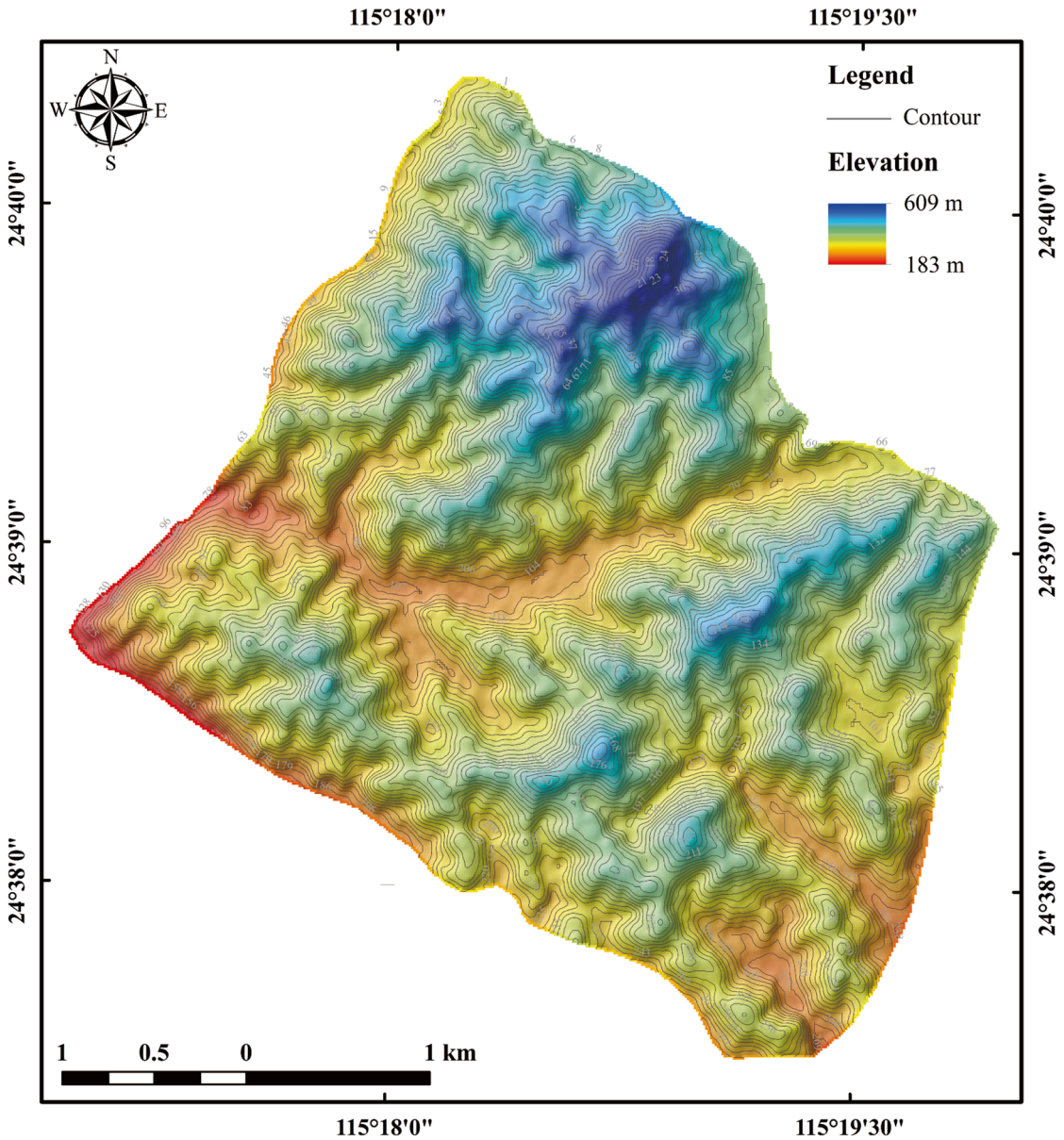

Fig. 2 Topographic characteristics of the study area (January 24, 2019)

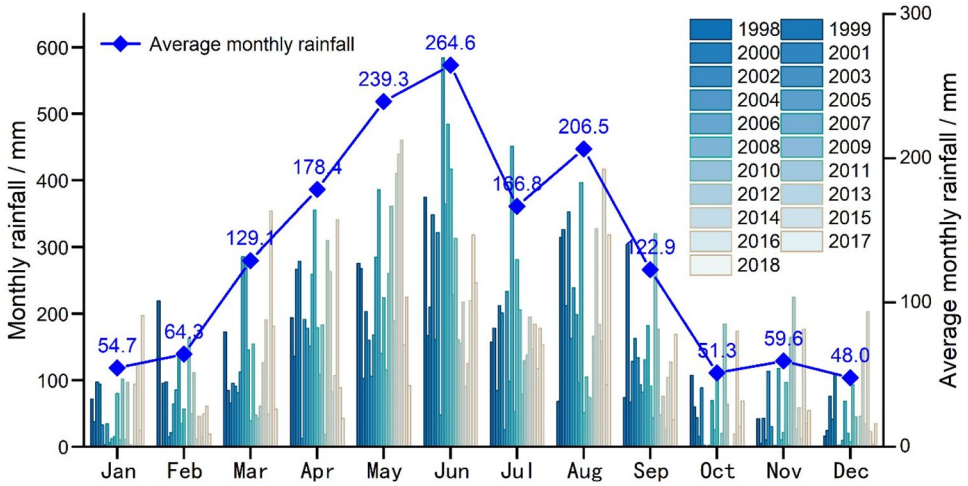

Fig. 3 Monthly rainfall and monthly average rainfall of Longchuan County from 1998 to 2018

north to south. The area with low mountains and hills accounts for more than 90% of the total area. The Meteorological Bureau of Longchuan County statistically analyzed the rainfall data for the whole county and obtained the monthly rainfall and monthly average rainfall of Longchuan County from 1998 to 2018, as shown in Fig. 3. Due to the subtropical monsoon climate, the annual rainfall in the study area exhibits bimodal characteristics. The first rainfall peak typically occurs in June, the monthly average rainfall reaches 264.6 mm, and the second rainfall peak occurs in August, with a monthly average rainfall of 206.5 mm. The above group-occurring landslide disaster event in Longchuan County was attributed to heavy rainfall occurring from June 10 to 13, 2019, which was observed during the first rainfall peak period in the region, generally conforming to the regional climate environment.

The Quaternary overburden in the study area mainly comprises granite residual soil (Q_4^{el}). Due to weathering differences, the thickness changes greatly. The thickness generally varies between 1 ~ 5 m and exceeds 8 m locally. The underlying bedrock comprises Paleozoic granite (Pz1), with notable weathering, a very thick fully weathered layer, and well-developed joints and fissures in both moderately and strongly weathered layers. The underground water mainly encompasses pore water in the loose accumulation layer. The underground water level changes with the terrain and is mainly supplied by rainfall. The underground water level increases considerably during the rainy season (March to September) and drops to the lowest level during the dry season (October to February of the following year). According to regional geological data and field surveys, there are no traces of geological structures, such as faults and folds, in the area, and the structural environment is very simple. Figure 4 shows the characteristics of the regional geological environment.

Spatial–temporal distribution characteristics

Spatial distribution

Upon reaching the hardest-hit area for the first time, the authors were deeply shocked by the devastated Mibei village. A large number of landslides had occurred. The road was blocked by unconsolidated landslide deposits, the river was silted by sediments, and the water level had risen, resulting in overland flow. The greatest impression of the hardest-hit area was that the mountains exhibited no complete form, and water flow did not occur along flow paths. According to the field survey results, the numerous landslides developed in Mibei village were small landslides. Even if certain landslides could form scar areas greater than 10,000 m^2, the maximum volume would be less than 100,000 m^3 because the landslide thickness is generally smaller than 5 m. To further analyze the spatial distribution characteristics of landslides in this region, the research group visually interpreted high-resolution postdisaster remote sensing images recorded on August 24, 2019, with a panchromatic band of 0.5 m and a multispectral band of 2 m, and statistically analyzed the relationship between important topographic factors and landslides combined with ALOS 12.5-m digital elevation model (DEM) data for the whole region.

There were 327 landslides in Mibei village (Fig. 5a), and the total scar area reached 75.25×10^4 m^2, accounting for more than 5% of the total area of Mibei village. Among these 327 landslides, the number of landslides with scar areas larger than 10,000 m^2 accounted for less than 5% of the total number of landslides, and the number of landslides with scar areas larger than 5000 m^2 occupied less than 14% of the total number of landslides. As the landslide thickness was generally smaller than 5 m, the total volume was almost less than 100,000 m^3, and even most of them were less than 20,000 m^3. This phenomenon indicates that the landslides caused by heavy rainfall exhibited the characteristics of small-scale and multipoint damage. Based on the plane characteristics of landslides (Fig. 5b), the landslides were widely distributed, mainly in the low mountainous area in the north of the Mibei River, followed by the X158 county road. The number of landslides was obviously small in the hilly area to the south of the Mibei River. The slope gradient in the low mountainous area is generally higher than 35°, with high gravitational potential energy, which constitutes the driving force condition for slope instability. In addition, the catchment conditions in the low mountainous area are relatively good, and the influence of ponding at the slope foot or channel water at the slope foot is

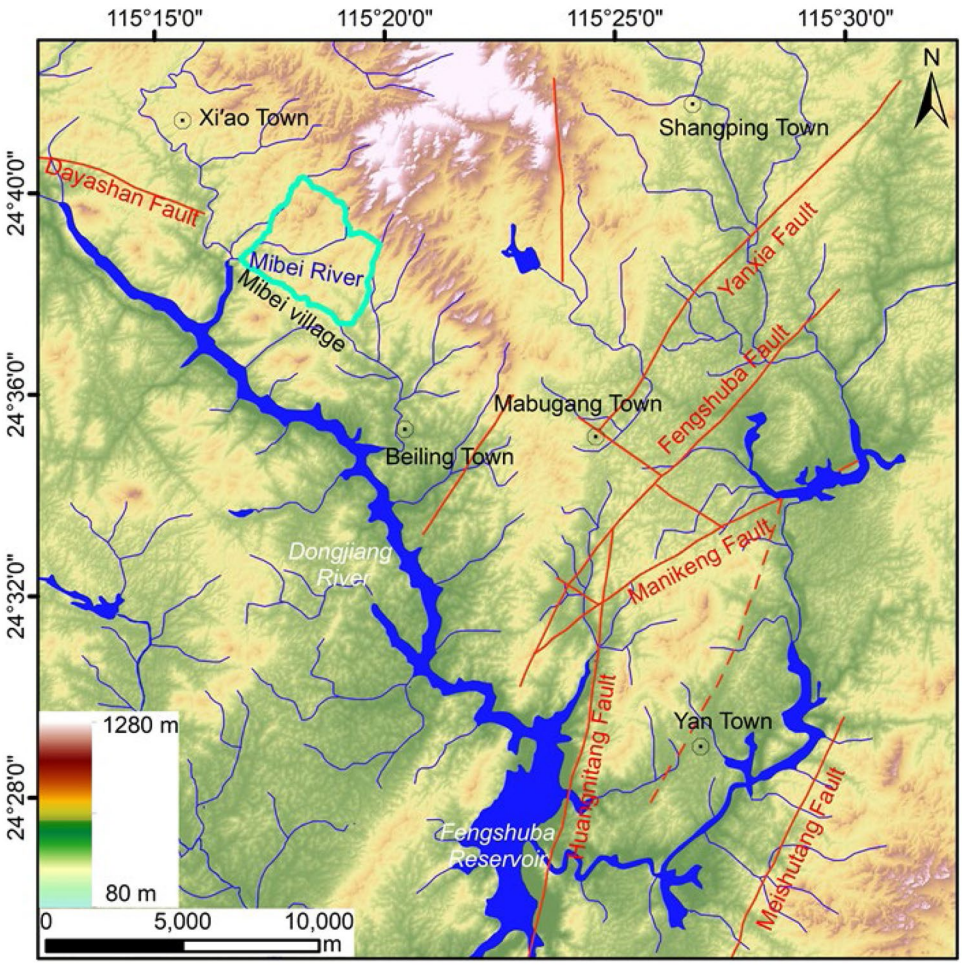

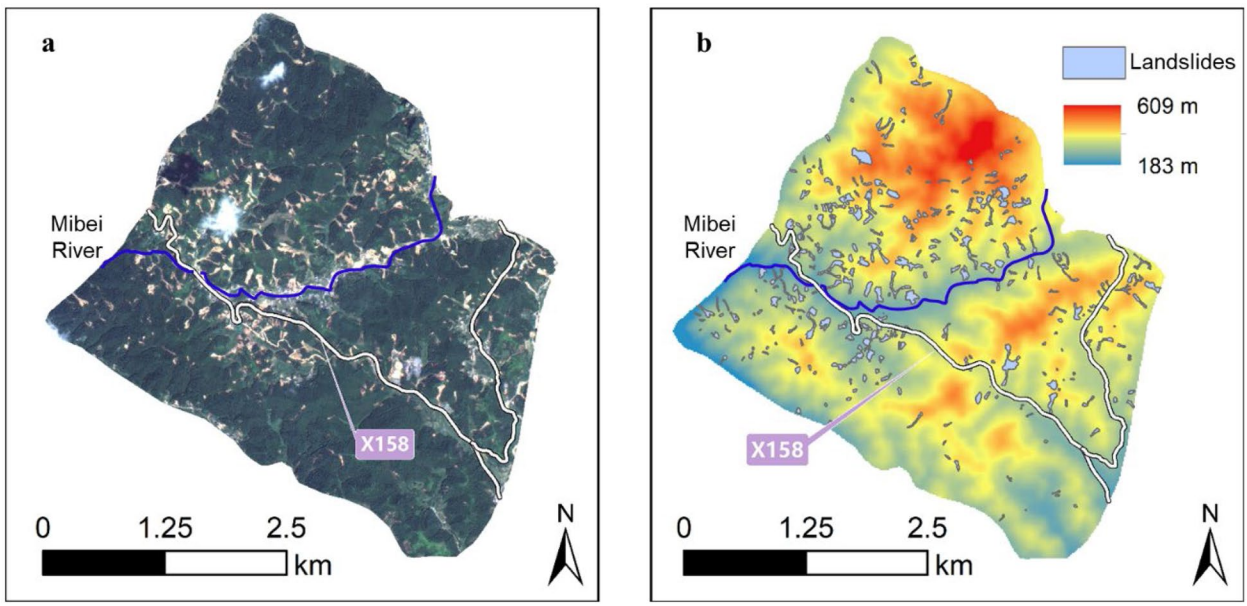

Fig. 4 Regional geological environment characteristics of the study area

Fig. 5 **a** Remote sensing image of Mibei village taken by Gaofen-1 on August 24, 2019; **b** remote sensing interpretation results of the landslides observed in Mibei village

prominent. Long-term immersion, softening, or erosion scouring is extremely unfavorable to the slope stability. The landslides distributed along the X158 county road were closely related to slope excavation. On the one hand, slope excavation generated high and steep free faces to provide spatial conditions for landslide formation. On the other hand, excavation reduced the anti-sliding force and stability of the slope. Under the action of continuous heavy rainfall, landslide disasters easily occurred. The unconsolidated landslide deposits occurring along the X158 county road also constituted the primary cause of postdisaster traffic blocking, notably impeding emergency rescue teams.

According to previous research results, terrain conditions in high mountainous areas significantly impact the distributions of light and rainfall, and slopes can therefore be divided into shady and sunny slopes. Under the influence of a complex terrain, there exists an inevitable relationship between the distribution pattern of rainfall-induced landslides and various terrain elements (Yu et al. 2016; Wang et al. 2019; Si et al. 2019). However, the study area exhibits a low mountainous and hilly terrain, and the maximum elevation difference only reaches 400 m. In this topographic environment, the rainfall distribution hardly yields notable influences. Therefore, this paper focuses on two factors, namely, the terrain slope and elevation. The terrain slope affects rainfall infiltration, and the elevation determines whether the slope achieves the potential energy conditions required for instability and failure. Based on the plane distribution characteristics of landslides, it has been preliminarily determined that there exists a certain relationship between the elevation and occurrence of landslides. Figure 6 shows the statistical relationship between the elevation, terrain slope, and landslide scar area. Landslides were mainly distributed in the elevation section from 300 ~ 400 m, and the dominant slope susceptible to landslides ranged from 35 ~ 45°. The higher the elevation in the study area, the more the slope gradient generally increases, especially near ridges, and the slope gradient could reach more than 60°. This topographic environment is not conducive to groundwater infiltration, and a large rainwater amount can produce groundwater flow. Therefore, the impact on the slope is relatively limited. With decreasing elevation, the terrain slope declines. For example, the terrain near the Mibei River is relatively flat, which is conducive to continuous rainfall infiltration, and the slope potential energy is low. Consequently, it is difficult to reach the potential energy conditions for instability initiation. Therefore, landslides were mainly concentrated in the medium-gradient section in terms of the terrain slope and elevation, which constituted the best comprehensive relationship between the terrain conditions and rainfall, resulting in the most well-developed landslides.

Temporal distribution

According to the disaster conditions at different time points, as revealed by local villagers, the landslide disaster in the study area not only exhibited the characteristics of a centralized distribution but also exhibited the phenomenon of centralized occurrence, and landslides mainly occurred from 20:00 on June 11 to 04:00 on June 13. This phenomenon was closely related to the rainfall structure. The study area experienced heavy rainfall many times from May to July 2019 (Fig. 7). Within longer than 1 month before the disaster, the maximum daily rainfall in the study area reached 57.3 mm, and the nearest heavy rainfall reached 55 mm (June 1). Thereafter, mostly rain-free conditions persisted for 7 days, and the surface water on the slope surface form the early rainfall dissipated greatly during this period. In an interview with local villagers, it was discovered that due to the relatively low rainfall intensity in the early stage, and on approximately June 7 after the rainfall, the shallow soil had recovered to its previous characteristics, and normal farming could be carried out. In addition, in the collected data, a construction site near Mibei village completed geotechnical test of granite residual soil on a slope on June 8, and the volumetric moisture content was 15 ~ 21%, which belonged to the natural volumetric moisture content under rain-free environment. The observed rainfall-induced group-occurring landslides were not directly related to the early rainfall event. After June 10, continuous heavy rainfall occurred in the study area for 4 consecutive days. The daily rainfall amount reached 153.5 mm on June 10, 72.2 mm on June 11, 33 mm on June 12, and 22.4 mm on June 13. The rainfall observed on the first 2 days was the highest, and the overall rainfall exhibited a gradual decreasing trend. According to the period of concentrated landslide occurrence, a large number of landslides occurred intensively after only 2 days of heavy rainfall, and the cumulative rainfall amount reached

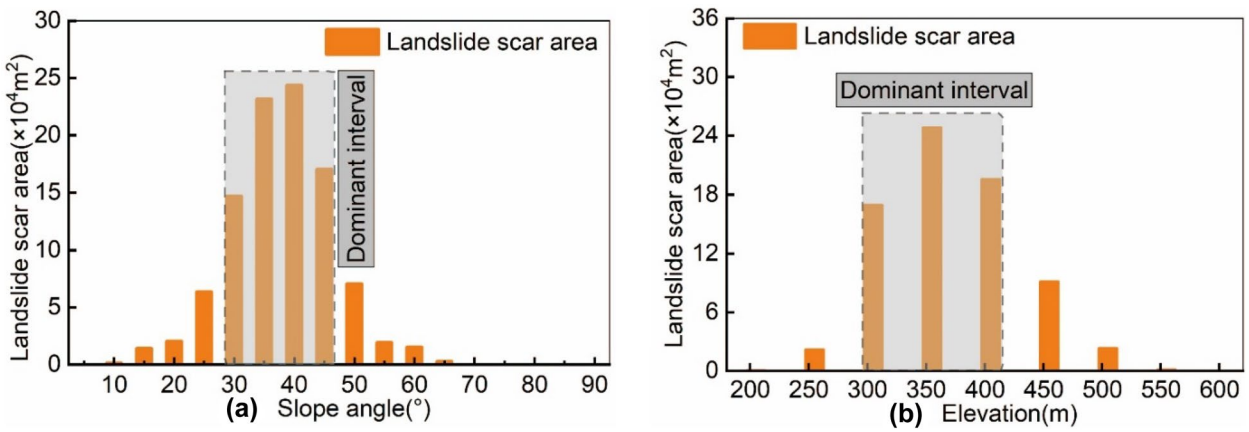

Fig. 6 Relationship between the landslide scar area (*LSA*), slope angle, and elevation: **a** slope angle; **b** elevation

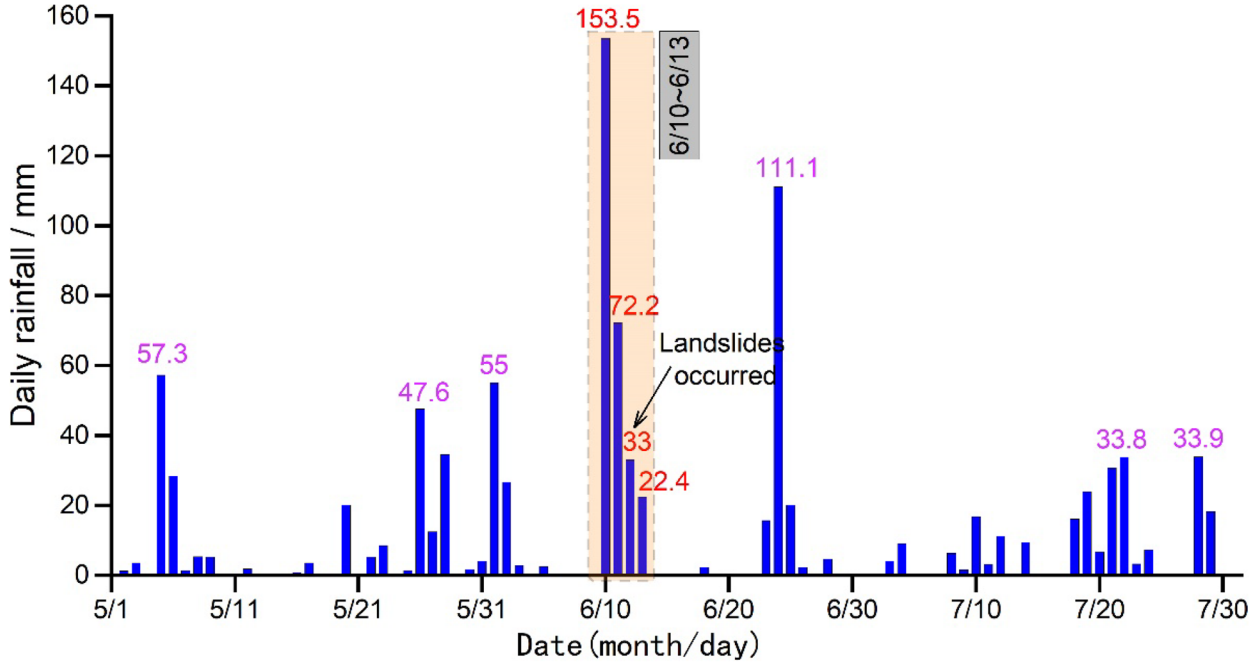

Fig. 7 Daily rainfall distribution in the study area from May to July 2019

as high as 225.7 mm. Therefore, it was preliminarily determined that the group-occurring landslides were mainly caused by continuous heavy rainfall from June 10 to 11.

Figure 8 shows the hourly rainfall distribution in the study area from June 9 to 13, 2019, which can further explain the relative temporal relationship between the observed group-occurring landslides and rainfall. From the early morning of June 10 to the end of rainfall at 18:00 on June 13, the hourly rainfall fluctuated throughout the whole process, and 4 hourly rainfall peaks successively occurred, with peak hourly rainfall amounts of 27, 20.7, 36.5, and 48.4 mm, all of which occurred before the occurrence of group-occurring landslides. A large number of landslides ensued just after the last hourly rainfall peak (20:00 on June 11). During the time interval of concentrated landslide occurrence, weather conditions without rain largely prevailed, and the maximum hourly rainfall was lower than 5.0 mm. However, the previous cumulative rainfall

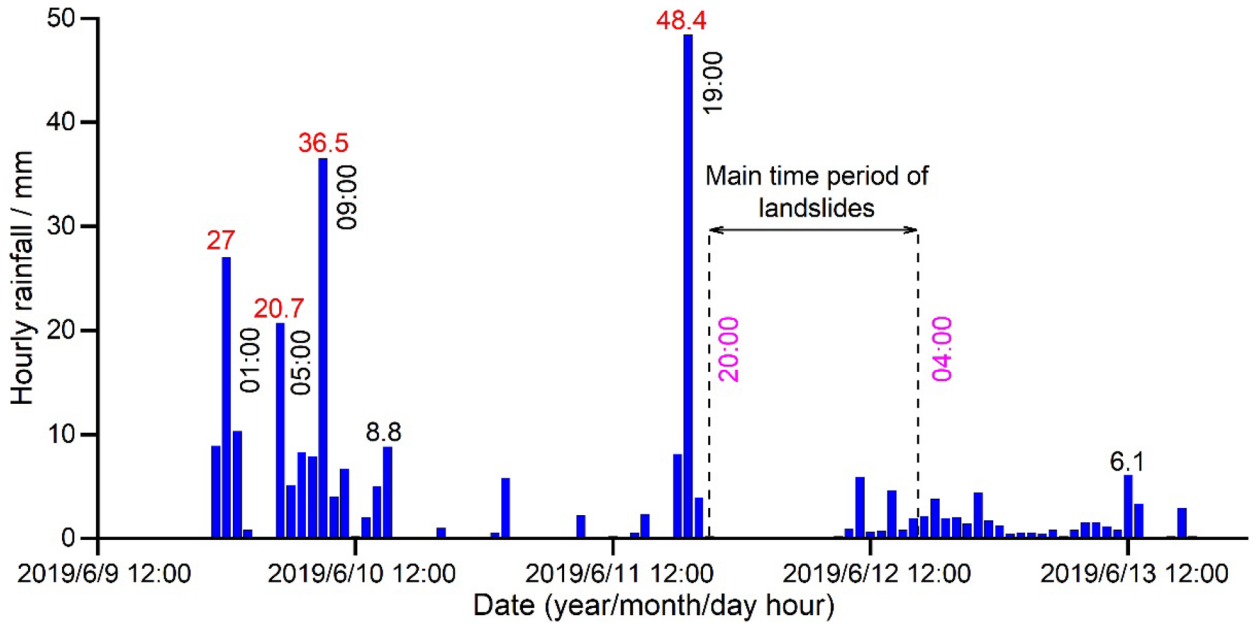

Fig. 8 Hourly rainfall distribution in the study area from June 9 to 13, 2019

amount reached 225.7 mm. The lag impact of rainfall on the slope seepage field and granite residual soil properties was thus revealed. Consequently, hundreds of landslides occurred within just 8 h.

Through the temporal relationship between the group-occurring landslides and rainfall structure, as shown in Figs. 7 and 8, it could be concluded that extreme heavy rainfall from June 10 to 11 was the key controlling factor of the disaster event, and it was further confirmed that granite residual soil landslides exhibit a major rainfall lag effect. In addition, the single-day rainfall in the study area exceeded 100 mm again on June 24, the rainfall intensity was slightly lower than that on June 10, and no large-scale landslide disaster ensued, which could be largely explained by an unsustainable rainfall structure.

Deformation characteristics and development process

According to the detailed field survey results, although hundreds of landslides occurred within the study area, the landslide characteristics were similar due to the similarity in geological environmental conditions. The landslides in the study area were mainly characterized by traction deformation and failure, and the plane characteristics were semicircular, tongue-shaped, strip-shaped, and other forms. The characteristics of the trailing edge and two sides of these damaging landslides were clear and easy to identify, and the position of the front shear outlet was mostly buried due to accumulation. After failure, a 1 ~ 2-m high steep ridge was formed at the trailing edge of the landslide, the depth of the sliding surface generally ranged from 1.5 ~ 3 m, and only a few landslides exhibited a thickness larger than 5 m. Due to traction deformation, the slope at the top of the trailing edge experienced varying degrees of tensile failure, and trees and bamboo plants at the top of the slope exhibited the characteristics of toppling deformation. Affected by the slope, the majority of the landslide mass moved toward the foot of the slope, and a large area of the sliding bed of the completely weathered layer or the moderately and strongly weathered layers became exposed, while a small fraction of the landslide material remained on the slope surface. The branches and roots of damaged and transported trees were interlocked and stacked.

To further analyze the failure characteristics and instability mode of the observed landslide disasters in the area, a representative landslide was selected for analysis. This landslide was located on the back mountain slope of the gathering area at the center of Mibei village, which was conducive to the detailed investigation at the site. The scale of the landslide was relatively large, the boundary was complete, and there were still deformation signs at the trailing edge. In addition, the landslide had a great impact, causing house damage and river siltation. The landslide mass was approximately 103 m long and 92 m wide. The thickness of the landslide mass ranged from approximately 2 ~ 5 m, with a total volume of 38,000 m^3. The landslide mainly comprised granite residual soil, which was a small landslide (Fig. 9a, b). A sliding surface developed along the granite eluvium and gradually cut

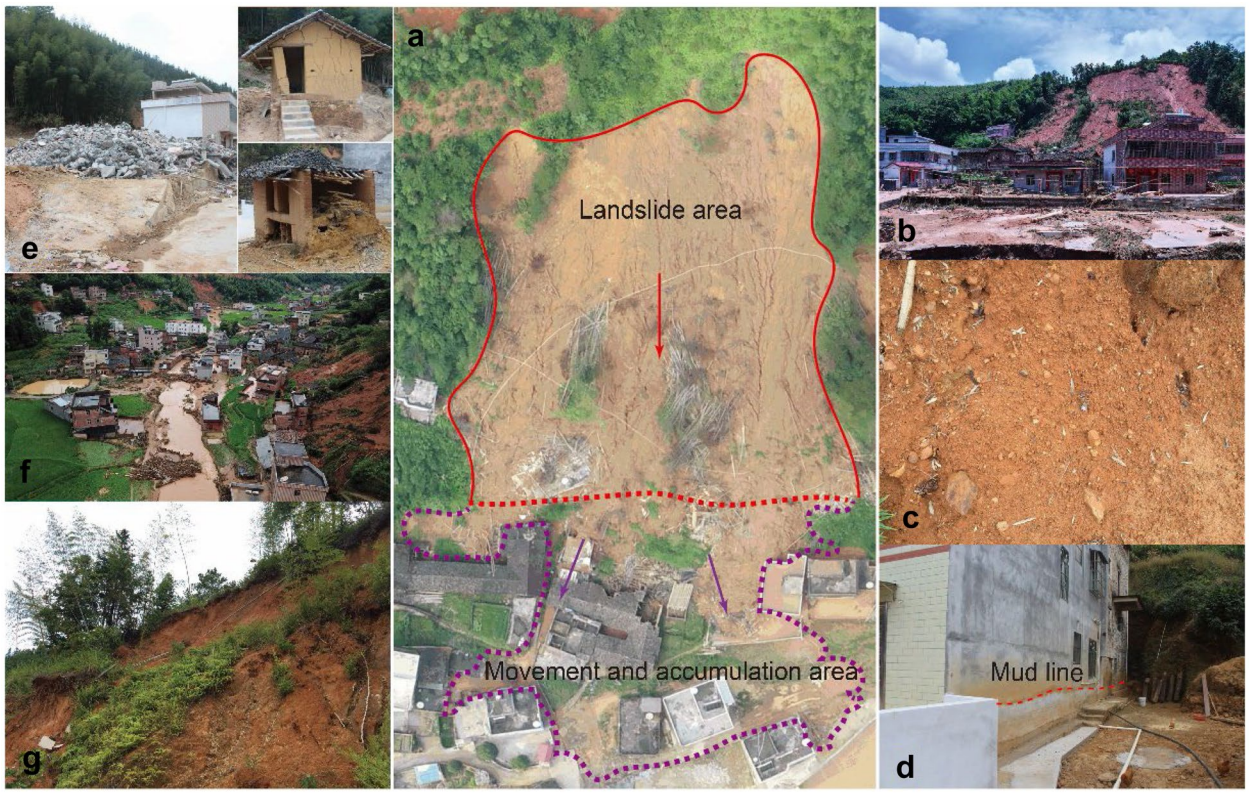

Fig. 9 Failure characteristics and influence results of a typical landslide. **a** Panoramic features of the landslide (UAV image); **b** front features of the landslide; **c** landslide deposits; **d** mud line in the movement and accumulation area; **e** damaged houses; **f** river siltation characteristics (UAV image); **g** deformation characteristics of the trailing edge

into the fully weathered layer near the front edge. Hence, accumulation mainly entailed silty clay mixed with a small amount of weathered residual breccia and gravel (Fig. 9c). In the high-rainfall environment from June 10 to 11, the slope became increasingly damaged. Due to the high-saturation state of the damaged loose soil, the flow characteristics of the unstable landslide were highly prominent in the movement process. The power provided by the gravitational potential energy endowed the landslide with a certain breaking force, resulting in burial or dislocation and cracking of the houses occurring in the residential area at the slope foot (Fig. 9d, e). Subsequently, continuous rainfall established a surface catchment, which further increased the moisture content in the loose accumulated deposits. These deposits continued to move forward from the gently sloping terrain at the foot of the slope toward the residential area, and soil and water increasingly separated, resulting in the accumulation of landslide materials in front of and behind the affected residential houses. Mud flowed into the Mibei River, which increased the water level of this river, and mud also reached the pavement and cultivated land (Fig. 9f). Traction deformation occurred along the trailing edge of the landslide due to free face conditions, resulting in tension cracks. Staggered deformation and even sliding failure ensued in certain sections under rainfall conditions from June 12 to 13, and trees and bamboo on the slope surface were displaced (Fig. 9g).

According to the deformation and failure characteristics of the considered group-occurring landslides and rainfall infiltration pattern, the development process of these landslides can be divided into 4 stages.

① Rainfall infiltration and unsaturated–saturated development state

At the initial rainfall stage, infiltration is the main factor promoting a continuous increase in the volumetric moisture content, and granite residual soil gradually develops from an unsaturated state to a saturated state. With increasing rainfall, the rainfall influence depth and range gradually increase. When the rainfall intensity is higher than the permeability of granite residual soil, some rainwater is transformed into surface water to scour and erode the slope surface.

② Formation and stability decline in the slope surface saturation zone

Under continuous rainfall infiltration, the slope surface gradually produces a saturation zone, and the scope of the saturation zone continues to expand and deepen. The volumetric moisture content in granite residual soil increases, the mechanical strength decreases, and the slope weight increases, resulting in an increase in sliding force and a decrease in the resisting force. Then, the slope stability tends to decrease.

③ Slope instability and impact failure

When the mechanical strength of granite residual soil is attenuated to the point where the slope stability can no longer be maintained, the landslide mass becomes unstable and damaged under the action of self-weight. The impact kinetic energy provided by the gravitational potential energy causes the landslide mass to displace any houses close to the front edge of the slope, causing these houses to become compressed and crack.

④ Fluidization movement and accumulation after instability

The speed of the landslide mass under movement inhibition rapidly decreases or some material accumulation occurs, and the remaining highly saturated landslide unconsolidated materials will bypass the impacted houses and continue to flow down along roads and ditches. In this process, water and soil are increasingly separated, a large amount of landslide materials accumulates in front of and behind the affected houses, and dilute mud or water flows into the Mibei River.

Initiation mechanism of landslides

Experimental scheme

To further research the initiation mechanism of granite residual soil slopes under continuous heavy rainfall, the research group selected a typical granite residual soil slope in the study area and created an in situ physical model through manual excavation. Moreover, a set of artificial rainfall simulation systems was independently designed, and the system was applied in artificial rainfall model tests.

The model exhibited an inclined length of 2.1 m, a width of 1.2 m, and a slope of 40°. A vertical section with a height of 30 cm was excavated at the front edge of the slope, and vegetation and rooted soil with a thickness of approximately 10 cm were removed from the slope surface. The whole model largely comprised granite residual soil, with a natural density of 1.6 g/cm^3, a dry density of 1.41 g/cm^3, and a saturated permeability coefficient of 10^{-3} cm/s, indicating a moderate permeability. The artificial rainfall system consisted of a microscale water pump, flowmeter, and rainfall nozzle, which could simulate the actual rainfall intensity. Figure 10a shows the overall characteristics of the model and artificial rainfall system. Two rows of rainfall nozzles were arranged in parallel with the model. Soil pressure and volumetric moisture content sensors were embedded along the central axis of the model, at burial depths of 30 and 80 cm, respectively. The two monitoring points were separated by an oblique distance of 100 cm, and the minimum oblique distance from the sensor to the excavation section reached 35 cm. Figure 10b shows the sectional features of the monitoring instrument layout. Due to the complex structure of the actual rainfall, artificial rainfall cannot simulate the effect of actual rainfall. In order to approach the actual rainfall structure to the greatest extent, the total rainfall is controlled and is consistent with the actual rainfall during the test, and the discontinuous characteristics in the actual rainfall structure are considered. The test lasted for 2 days, with a daily rainfall of 9 h and a total of 18 h. The cumulative rainfall was 270 mm, so the average rainfall intensity was 15 mm/h. No rainfall was simulated for 14 h between the two rainfall processes, which represented the discontinuity in the actual rainfall structure. In addition, to observe the characteristics of rainfall infiltration, blue indicator dye was added to the water to study the characteristics of the groundwater seepage path.

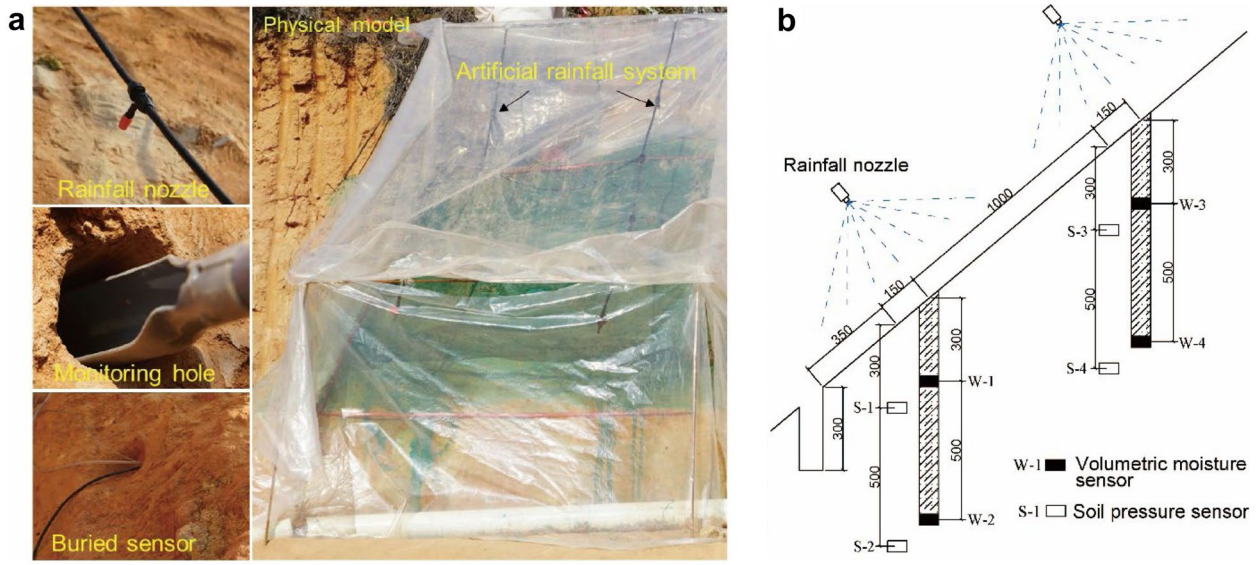

Fig. 10 **a** Physical experimental model and related facilities; **b** sensor layout section inside the model

Research findings

Figure 11 shows the time-history curve of the volumetric moisture content at the different locations under 2-day rainfall conditions. During the first 5 h of the rainfall process on the first day, the volumetric moisture content recorded by the #1 and #3 sensors at a depth of 30 cm did not change significantly. After 5 h of rainfall, the monitoring data recorded by the #1 volumetric moisture content sensor gradually increased and exhibited an accelerated growth trend. By the end of the rainfall process on the same day, the volumetric moisture content had increased to 24.6%, and the growth trend was nearly vertical. The #3 volumetric moisture content sensor indicated a gradual growth trend as a whole, with limited rapid growth approximately 20 min before the end of the rainfall process on the same day. The rainfall process on the first day was stopped at 18:00, and the rainfall process on the second day was initiated at 08:00. No rainfall was simulated in between, and the process lasted 14 h. After the rainfall process on the second day, sensors #1 and

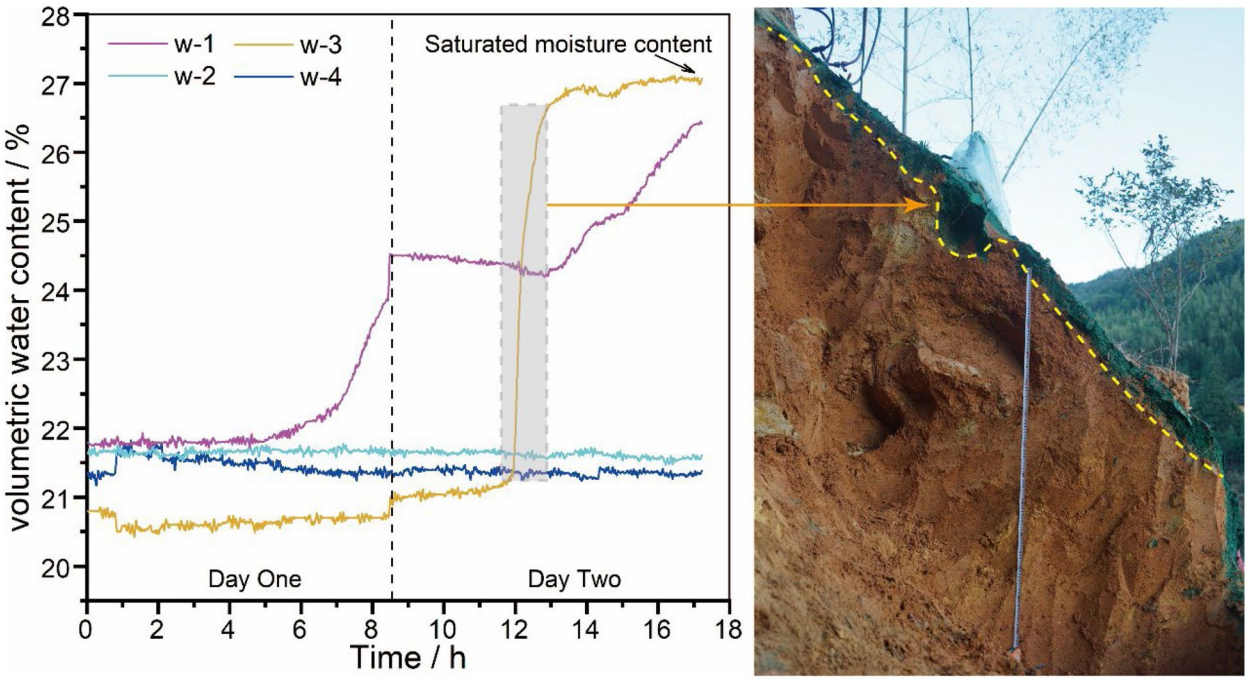

Fig. 11 Time-history curve of the volumetric water content and characteristics of the seepage section

#3 did not immediately indicate a growth trend of the volumetric moisture content, and the volumetric moisture content recorded by sensor #1 even exhibited a small decrease. This phenomenon was caused by the evaporation and seepage movement of pore water during the rainfall-free period. The rainfall process on the second day compensated for the pore water loss during the rainfall-free period. The data characteristics fully reflected the change trend of the slope volumetric moisture content in the actual rainfall process. After 3.5 h of rainfall on the second day, sensor #3 first increased and indicated a sharp increasing trend. The volumetric moisture content increased from 21.3 to 26.8% over approximately 1 h and then stabilized at approximately 27%. Sensor #1 again indicated continuous growth after 4.5 h of rainfall, and the volumetric moisture content reached 26.3% at the end of the rainfall process on the second day, but a stable value was not reached. Based on the excavation section after the test, it was found that the test physical model remained uneven. There occurred a stone block with a diameter of approximately 20 cm above sensor #3. The stone block was covered by the surrounding residual soil, resulting in slow rainfall infiltration at the early stage. The infiltrated pore water moved around the stone block, thereby increasing the seepage path, resulting in a lag in the reaction of sensor #3 behind that of sensor #1. In the whole rainfall process, the data recorded by sensors #2 and #4 at a depth of 80 cm did not change notably. Artificial rainfall imposed the greatest influence on the soil below the model. This phenomenon was closely related to the rainfall intensity and overburden permeability. This conclusion could also explain why the group-occurring landslides in the study area mostly involved shallow surface failure.

According to the characteristics of the excavation section after the test, as shown in Fig. 11, the local volumetric moisture content exhibited a differential distribution due to the influence of impurities (stone blocks). In regard to the whole model, the migration process and distribution of pore water after rainfall infiltration were regular, revealing shallow characteristics at the top and notable characteristics at the bottom. The pore water seepage depth in the middle and lower parts of the model was relatively large, while the pore water seepage depth in the upper part of the model was relatively small, which was attributable to pore water seepage toward the front under the action of the gravitational potential energy after the model surface had become saturated. An uneven pore water distribution could also cause differences in the deformation and failure characteristics of the model. Under the influence of rainfall, the soil in the middle and lower shallow layers of the model occurred in a saturated state, and the shear strength greatly decreased, resulting in a decline in the stability and gradual failure of the middle and lower parts of the model. Because the influence depth of short-term heavy rainfall was limited and the rainfall intensity was much higher than the soil permeability coefficient, the influence of heavy rainfall was mainly concentrated in the shallow surface zone. Moreover, surface water flow increased at the later rainfall stage, and the erosion effect on the surface of the model was strengthened, thus forming the deformation and failure characteristics depicted in Fig. 12.

Due to the limited influence depth of rainfall on the first day, the soil pressure at the different locations did not change considerably. In the rainfall process on the second day, with increasing rainfall impact, shallow surface sliding failure or surface water erosion

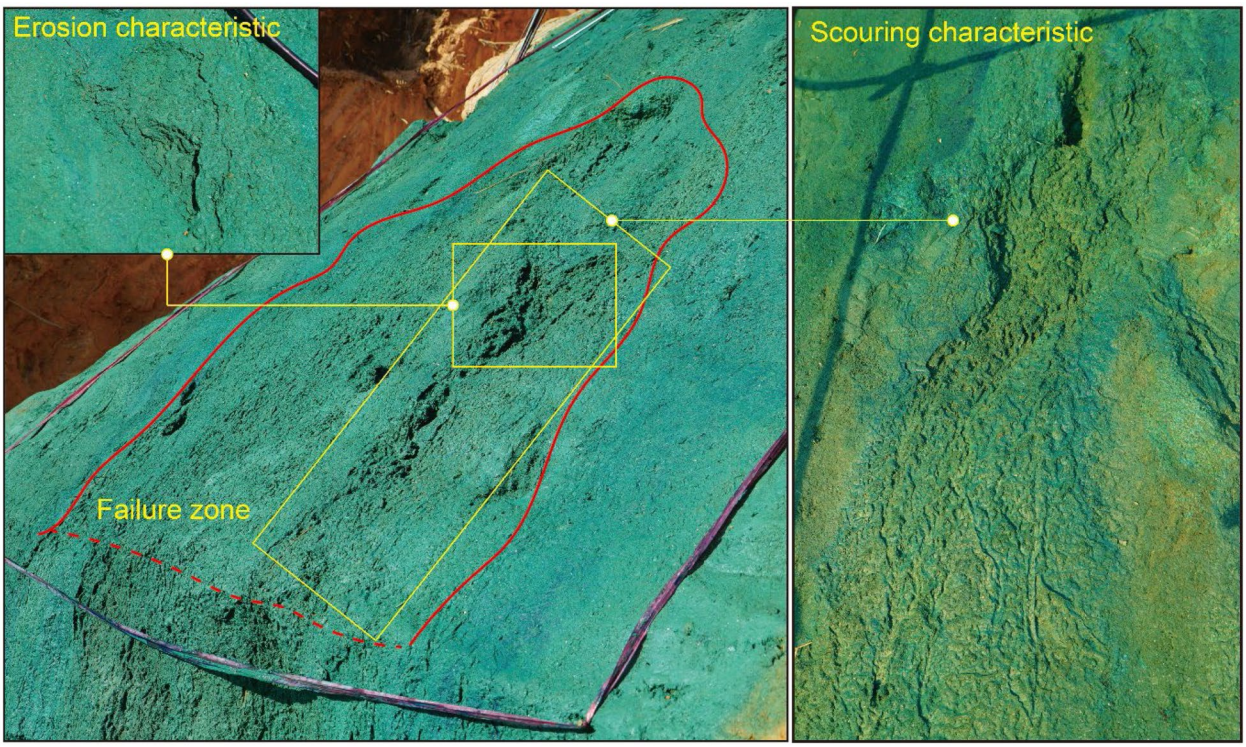

Fig. 12 Sliding failure characteristics of the middle and lower parts of the model

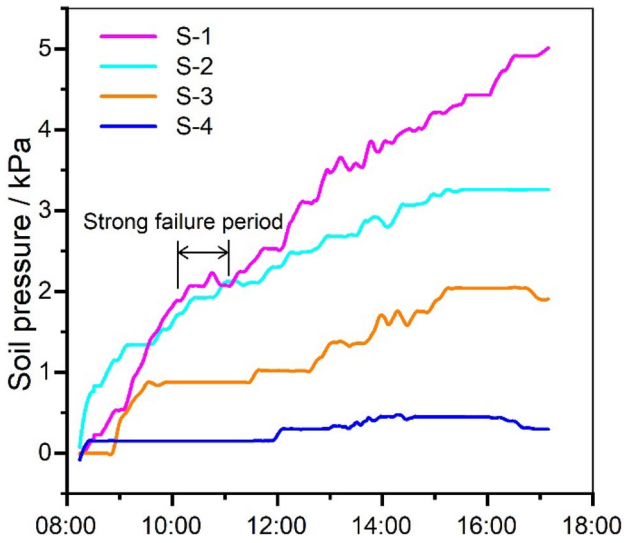

Fig. 13 Time-history curve of the soil pressure on the second day

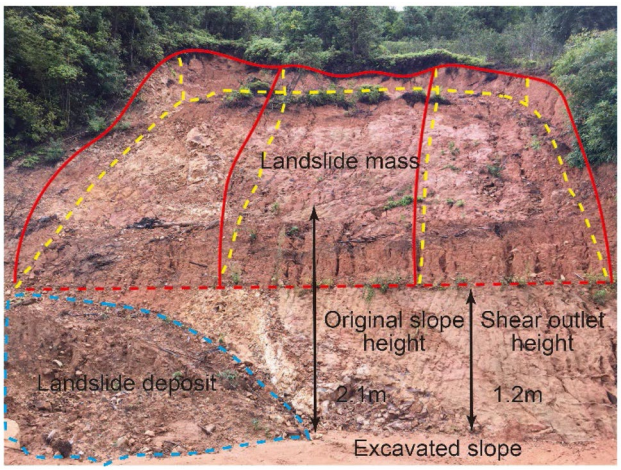

Fig. 14 Failure characteristics of the excavated slope

failure occurred on the surface of the model, and the soil pressure at each position further indicated an obvious development trend (Fig. 13). Since rainfall infiltration mainly affected the middle and lower parts of the model and the gravitational potential energy increased upon soil moisture content enhancement, the growth range of the #1 and #2 soil pressure sensors was the largest and exhibited a continuous growth trend. The soil pressure at sensor #1 finally reached 5.1 kPa, and the soil pressure at sensor #2 remained stable at 3.2 kPa after 7 h of rainfall. Since the rainfall influence depth in the upper part at sensor #3 was relatively limited, the soil pressure at sensor #3 approached 2.0 kPa at the end of the test. Sensor #4 exhibited a large burial depth and a small rainfall infiltration depth in the upper part, and sensor #4 consequently imposed no notable influence of the slight change in soil pressure. The soil pressure response at the different depths and locations reflected the nonuniformity of the impact of rainfall on the model. The higher the rainfall infiltration and the larger the infiltration depth were, the stronger the earth pressure response. In contrast, the soil pressure response was limited or no response was observed. Moreover, sliding failure of the slope surface could reduce the overburden load on the soil pressure gauge. After failure, the volumetric moisture content in the soil in the lower part of the exposed surface was slightly lower than that at the slope surface, and rainfall infiltration easily ensued. Therefore, while the overburden load was reduced, continuous rainfall infiltration compensated for the reduction, which resulted in a gradual growth or stagnation state in the monitoring curve.

Comprehensive analysis revealed that rainfall is the controlling factor of landslide disasters. Due to the physical properties of granite residual soil, the influence depth of heavy rainfall is limited. Under the influence of heavy rainfall, the shallow surface layer of a given slope gradually reaches the saturation state. On the one hand, an increase in pore water causes a continuous reduction in the soil mechanical strength, which leads to a decline in the slope stability. On the other hand, when the shallow surface layer of the slope becomes completely saturated, a saturated seepage field is established, and pore water seeps and accumulates at the foot of the slope under the action of the gravitational potential energy. Furthermore, the excavation section revealed that the influence depth of rainfall in the middle and lower parts of the model is larger than that in the upper part, and an uneven pore water distribution determines that deformation and failure are concentrated in the shallow surface zone in the middle and lower parts. In regard to the excavated slope, the formation of a free face reduced the leading edge anti-sliding resistance to a certain extent. Compared to the original slope, the stability of the excavated slope was reduced, and the superposition effect of rainfall resulted in a higher susceptibility of the slope to instability and failure, as shown in Fig. 14. In this disaster event, a large number of landslides occurred along the X158 county road. The free slope formed by highway excavation was a prerequisite for landslide occurrence in this disaster event, and on this basis, heavy rainfall directly caused this disaster.

Conclusions

Based on detailed investigation results obtained in Mibei village, Beiling town, combined with satellite remote sensing images, rainfall monitoring data, and artificial rainfall physical model tests, in this paper, the temporal and spatial distribution patterns and disaster mechanism of mass disasters in granite areas were studied. A total of 327 landslides occurred in Mibei village, Beiling town, due to continuous heavy rainfall from June 10 to 13, 2019, and these landslides were mainly distributed in low mountainous areas, followed by the X158 county road. Sections at an elevation ranging from 300 ~ 400 m and a slope ranging from 35 ~ 45° were the most susceptible to landslides. Topographic changes affect the comprehensive relationship between precipitation, surface water, and groundwater and thus control the development degree of landslides. The observed landslides in the study area exhibited the characteristics of centralized occurrence (20:00 on June 11 to 04:00 on June 13). The cumulative rainfall amount on June 10 and 11 reached as high as 225.7 mm, which was the key to inducing mass landslides. The rainfall intensity and rainfall structure were the main causes of the occurrence of the large number of landslides, and these group-occurring landslides exhibited a notable rainfall lag.

The overall geological environment characteristics of the study area are relatively consistent, and the deformation and failure characteristics of the numerous landslides considered are highly similar. These landslides mainly involve small-scale traction sliding failure, and the thickness of the sliding body mostly ranges from 1.5 ~ 3 m. The flow pattern characteristics of the unconsolidated landslide material after failure are obvious. According to the deformation and failure characteristics of landslides and rainfall infiltration pattern, the development process of landslides is divided into four stages: ① rainfall infiltration and unsaturated–saturated state development, ② formation and stability decline in the slope surface saturation zone, ③ slope collapse and impact failure, and ④ fluidization movement and accumulation after instability. Because the rainfall intensity is much higher than the permeability coefficient of granite residual soil, heavy rainfall mainly affects the shallow surface zone of the slope, and non-infiltrated rainwater generates surface runoff, which is also the reason why group-occurring landslides are mainly characterized by shallow surface sliding failure. A saturated seepage field is produced in the shallow surface saturation area of the slope, which evolves into uneven distribution characteristics whereby the thickness of the saturation zone in the middle and lower parts of the slope is larger than that in the upper part under the action of the gravitational potential energy. Moreover, attenuation of the mechanical strength of the saturated soil can lead to a decline in the slope stability. As a result, deformation failure is largely observed in the middle and lower parts of the slope during heavy rainfall, and deformation can develop toward the upper part of the slope under the action of traction. Regarding excavated slopes, the slope anti-sliding force is reduced due to excavation, and suitable free face conditions increase the slope susceptibility to sliding failure under the influence of heavy rainfall.

Acknowledgements

We would like to thank the emergency department of the Nonferrous Mine Geological Disaster Prevention Center of Guangdong Province for providing geological data and disaster data, the Meteorological Bureau of Longchuan County for providing rainfall data, and Google Earth for providing remote sensing images. At the same time, we thank the local residents for their help in the field research process. Their support has made our field work complete smoothly. Finally, we also thank the anonymous referees and the editor for their constructive feedback and suggestions that encourage us to improve the quality of this paper.

Funding

This research is financially supported by the National Natural Science Foundation of China (Grant No. 41977252, U2005205), The Team Project of Independent Research of SKLGP (Grant No. SKLGP2020Z001), Opening Foundation of Key Laboratory of Geohazard Prevention of Hilly Mountains, Ministry of Natural Resources (Fujian Key Laboratory Of Geohazard Prevention) (Grant No. FJKLGH2021K006), and The Research Project of Nonferrous Mine Geological Disaster Prevention Center of Guangdong Province.

Declarations

Conflict of interest The authors declare no competing interests.

References

An R, Kong L, Li C, Luo X (2020) Strength attenuation and microstructure damage of granite residual soils under hot and rainy weather. Chin J Rock Mech Eng 39(09):1902–1911. https://doi.org/10.13722/j.cnki.jrme.2020.0073

Bai H, Feng W, Yi X, Fang H, Wu Y, Deng P, Dai H, Hu R (2021) Group-occurring landslides and debris flows caused by the continuous heavy rainfall in June 2019 in Mibei Village, Longchuan County, Guangdong Province, China. Nat Hazards 108(03):3181–3201. https://doi.org/10.1007/s11069-021-04819-1

Chen X, Zhou Q, Cai X (2011) Physical properties and shear strength characteristics of high liquid limit granite residual soil. Chin J Geotech Eng 33(06):901–908

Ding L, He B, Zhang D (2020). Investigation and reflection on "June 17, 2019" mountain flood disaster in Lingyun county, Baise city, Guangxi province. China Flood & Drought Management. https://doi.org/10.16867/j.issn.1673-9264.2020182

Gutierrez-Martin A (2020) A GIS-physically-based emergency methodology for predicting rainfallinduced shallow landslide zonation. Geomorphology 359. https://doi.org/10.1016/j.geomorph.2020.107121

Gutierrez-Martin A, Millan-Martin JP, Castedo R, Yenes JI (2021) Calculation of micropiles and anchors to reinforce a slope in emergency situations: application in Málaga, Spain. Geomatics Nat Hazards Risk 12(1):716–740. https://doi.org/10.1080/19475705.2021.1887373

Herrada MA, Gutierrez-Martin A, Montanero JM (2014) Modeling infiltration rates in a saturated/unsaturated soil under the free draining condition. J Hydrol 515:10–15. https://doi.org/10.1016/j.jhydrol.2014.04.026

Jian W, Huang C, Luo Y, Nie W (2020) Experimental study on wetting front migration induced by rainfall infiltration in unsaturated eluvial and residual soil. Rock Soil Mech 41(04):1123–1133. https://doi.org/10.16285/j.rsm.2019.0491

Jian W, Hu H, Luo Y, Tang Y (2017) Experimental study on deterioration of granitic residual soil strength in wetting-drying cycles. J Eng Geol 5(03):592–597. https://doi.org/10.13544/j.cnki.jeg.2017.03.003

Luo Y, He S, He J (2014) Effect of rainfall patterns on stability of shallow landslide. Earth Sci - J China Univ Geosci 39(09):1357–1363. https://doi.org/10.3799/dqkx.2014.118

Liu Y, Wen M, Su Y, Xu F (2016) Characteristics of geo-hazards induced by typhoon rainstorm and evaluation of geo-hazards early warning. Hydrogeol Eng Geol 43(05):119–126. https://doi.org/10.16030/j.cnki.issn.1000-3665,2016.05.18

Liu M, Zhou M, Zhang Y, Zhang T (2018) Development features of geological disasters in Taishun county, Zhejiang province during typhoon "Soudelor." East China Geol 39(01):66–72. https://doi.org/10.16788/j.hddz.32-1865/P.2018.01.009

Li C, Kong L, Shu R, An R, Zhang X (2020) Disintegration characteristics in granite residual soil and their relationship with the collapsing gully in South China. Open Geosci 12(01):1116–1126. https://doi.org/10.1515/geo-2020-0178

Liu W, Song X, Luo J, Hu L (2020a) The processes and mechanisms of collapsing erosion for granite residual soil in southern China. J Soils Sediments 20(02):992–1002. https://doi.org/10.1007/s11368-019-02467-4

Liu W, Song X, Huang F, Hu L (2019) Experimental study on the disintegration of granite residual soil under the combined influence of wetting-drying cycles and acid rain. Geomat Nat Haz Risk 10(01):1912–1927. https://doi.org/10.1080/19475705.2019.1651407

Liu W, Wan S, Luo X, Fu M (2020b) Experimental study of suffusion characteristics within granite residual soil controlling inflow velocity. Arab J Geosci 13(22):1–8. https://doi.org/10.1007/s12517-020-06193-x

Pan Y, Jian W, Li L, Lin Y, Tian P (2020) A study on the rainfall infiltration of granite residual soil slope with an improved Green-Ampt model. Rock Soil Mech 41(08):2685–2692. https://doi.org/10.16285/j.rsm.2019.1734

Si M, Cao J, Yang H (2019) Advances in research on the effects of micro-topography changes on surface hydrological processes. Chin J Eco-Agric 27(10):1587–1595. https://doi.org/10.13930/j.cnki.cjea.190505

Wang H (2011) Stability analysis and nonlinear prediction of granite residual soil slopes in Chu Chiang delta. Jilin University, Changchun
Wen Y, Yang G, Tang L, Xu C, Huang Z, Huang Z, Zhang Y (2016) Tests and parameters study of mechanical properties of granite residual soil in Guangzhou area. Rock Soil Mech 37(S2):209–215. https://doi.org/10.16285/j.rsm.2016.S2.025
Wang J, Zhang M, Ren S, Wang X, Miao C (2019) Simulation study on the impact of Taihang mountain slopes on downhill front cyclone rainstorm. Adv Earth Sci 34(07):717–730. https://doi.org/10.11867/j.issn.1001-8166,2019.07.0717
Xu X (2015) Research on the response and failing process of unsaturated residual soil slope under rainfall infiltration. Fuzhou University, Fuzhou
Yi X, Feng W, Bai H, Shen H, Li H (2021) Catastrophic landslide triggered by persistent rainfall in Sichuan, China: August 21, 2020, Zhonghaicun landslide Landslides 18(8):2907–2921. https://doi.org/10.1007/s10346-021-01701-w
Yang H, Yang T, Zhang S, Zhao F, Hu K, Jiang Y (2020) Rainfall-induced landslides and debris flows in Mengdong Town, Yunnan Province, China. Landslides 17(04):931–941. https://doi.org/10.1007/s10346-019-01336-y
Yang L, Ye L, Yu B, Wu Z, Deng J, Zhao B, Liu Q, Chen W (2021) Analysis of "5.16" rainstorm and flood and flash flood disaster prevention in the back mountain of Sanming city, Fujian province. J China Hydrol 41(03):95–100. https://doi.org/10.19797/j.cnki.1000-0852.20200031
Yu B, Wang T, Zhu Y (2016) Research on the topographical and rainfall factors of debris flows caused by shallow landslides. Adv Water Sci 27(04):542–550. https://doi.org/10.14042/j.cnki.32(1309),pp.04,2016.008

Wenkai Feng · Huilin Bai (✉)
State Key Laboratory of Geohazard Prevention and Geoenvironment Protection, Chengdu University of Technology, Chengdu 610059, China
Email: 553884932@qq.com

Wenkai Feng · Huilin Bai · Zhongteng Wu
Key Laboratory of Geohazard Prevention of Hilly Mountainous, Ministry of Natural Resources, Fuzhou 350002, China

Wenkai Feng · Huilin Bai · Zhongteng Wu
Fujian Key Laboratory of Geohazard Prevention, Fuzhou 350002, China

Bing Lan · Yiying Wu · Liangzheng Yan · Xinjun Ma
Nonferrous Mine Geological Disaster Prevention Center of Guangdong Province, Guangzhou 510062, China